

Structural phase transition study of the morphotropic phase boundary compositions of
 $\text{Na}_{0.5}\text{Bi}_{0.5}\text{TiO}_3\text{-PbTiO}_3$

This article has been downloaded from IOPscience. Please scroll down to see the full text article.

2009 J. Phys.: Condens. Matter 21 375902

(<http://iopscience.iop.org/0953-8984/21/37/375902>)

View [the table of contents for this issue](#), or go to the [journal homepage](#) for more

Download details:

IP Address: 129.252.86.83

The article was downloaded on 30/05/2010 at 05:05

Please note that [terms and conditions apply](#).

Structural phase transition study of the morphotropic phase boundary compositions of $\text{Na}_{0.5}\text{Bi}_{0.5}\text{TiO}_3\text{-PbTiO}_3$

Sarab Preet Singh¹, Rajeev Ranjan², Anatoliy Senyshyn³,
Dmytro Trots⁴ and Hans Boysen⁵

¹ Department of Physics, Indian Institute of Technology Delhi, New Delhi-110016, India

² Department of Materials Engineering, Indian Institute of Science, Bangalore-560012, India

³ Institute for Materials Science, Darmstadt University of Technology, Petersenstrasse 23, D-64287, Darmstadt, Germany

⁴ HasyLab/DESY, Notkestrasse 85, 22607 Hamburg, Germany

⁵ Department für Geo- und Umweltwissenschaften, Sektion Kristallographie, Ludwig Maximilians Universität, Am Coulombwall 1, 85748 Garching, München, Germany

E-mail: rajeev@materials.iisc.ernet.in

Received 24 April 2009, in final form 15 July 2009

Published 17 August 2009

Online at stacks.iop.org/JPhysCM/21/375902

Abstract

Neutron, synchrotron x-ray powder diffraction and dielectric studies have been performed for morphotropic phase boundary (MPB) compositions of the $(1-x)\text{Na}_{1/2}\text{Bi}_{1/2}\text{TiO}_3\text{-}x\text{PbTiO}_3$ system. At room temperature, the MPB compositions ($0.10 < x \leq 0.15$) consist of a mixture of rhombohedral (space group $R3c$) and tetragonal (space group $P4mm$) structures with the fraction of tetragonal phase increasing with increasing PbTiO_3 content. On heating, while the rhombohedral phase just outside the MPB region, i.e. $x = 0.10$, transforms directly to a cubic phase, the rhombohedral phase of the MPB compositions transforms gradually to a tetragonal phase, until interrupted by a rhombohedral–cubic phase transition. The correspondence of the dielectric anomalies with the structural transitions of the different compositions has been examined and compared with earlier reports.

(Some figures in this article are in colour only in the electronic version)

1. Introduction

Morphotropic phase boundary (MPB) ferroelectric solid solutions are attractive systems because of their technological significance in the area of transducer and actuator related applications [1–3]. Due to its superior properties, the most important solid solution system in this category is $\text{Pb}(\text{Zr}_{1-x}\text{Ti}_x)\text{O}_3$ (PZT). The interesting compositions of PZT lie around $x = 0.50$, where a MPB separates the rhombohedral and tetragonal phase fields [2]. Subsequent studies have claimed the presence of monoclinic phases for the MPB composition of PZT [4, 5]. A monoclinic phase is believed to provide a low energy pathway for the rotation of polarization on application of an external electric field, leading to an enhanced piezoelectric response [3]. Different types of monoclinic phases have also been reported in the MPB region of other related systems such as $\text{Pb}(\text{Mg}_{1/3}\text{Nb}_{2/3})\text{O}_3\text{-PbTiO}_3$

(PMN–PT) [6–9] and $\text{Pb}(\text{Zn}_{1/3}\text{Nb}_{2/3})\text{O}_3\text{-PbTiO}_3$ (PZN–PT) systems [9, 10]. However unlike for the PZT system, the parent compounds PMN and PZN are relaxor ferroelectrics. The large electrostriction associated with relaxor ferroelectrics make them technologically unique for development of a hysteresis free electric field strain response, which is an important criterion for micro-positioning related applications.

$\text{Na}_{1/2}\text{Bi}_{1/2}\text{TiO}_3$ (NBT) is a complex rhombohedral (space group $R3c$) perovskite which is known for its relaxor ferroelectric features. Its dielectric properties and structural phase transition behaviour have been investigated extensively over the years [11–18]. Owing to its rhombohedral structure, and associated ferroelectric properties, solid solutions of NBT with other ferroelectric perovskites have been investigated with the expectation to develop new MPB systems [19–30]. Of these, solid solutions with BaTiO_3 (BT) [19–22], PbTiO_3 (PT) [23–27] and KNbO_3 [30, 31] are particularly interesting

since they give features of MPB. Although interesting piezoelectric and pyroelectric properties of $\text{Na}_{1/2}\text{Bi}_{1/2}\text{TiO}_3\text{-PbTiO}_3$ (NBT-PT) have been reported in the past [24, 32], there is still a limited understanding of the structural phase transition behaviour of the MPB compositions of this system. Park and Hong [25, 26] have suggested that the MPB would lie in the composition range $0.13 < x < 0.15$. Elkechai *et al* [23] have reported existence of biphasic region in the composition range $0.10 < x < 0.20$, and have studied structural phase transitions only for compositions outside the MPB region. In view of the importance of the MPB compositions, it is important to have a detailed understanding of their structural phase transition behaviour. In this paper we have reported the results of the detailed structural and phase transition behaviour of the MPB compositions of the NBT-PT system and have examined the correspondence between the dielectric anomalies and the structural changes of this system. While confirming the two-phase (rhombohedral ($R3c$) + tetragonal ($P4mm$)) nature of the MPB, it is shown that the MPB compositions invariably exhibit transformation of the rhombohedral ($R3c$) phase to the tetragonal ($P4mm$) phase on heating until interrupted by the rhombohedral-cubic transition.

2. Experimental details

NBT-PT compositions were prepared by a conventional solid state reaction method. Stoichiometric amounts of high purity (>99.5%) Na_2CO_3 , PbCO_3 , Bi_2O_3 , TiO_2 were mixed in planetary ball mill for 6 h. The powders were placed in zirconia jars, containing zirconia balls, and acetone was used as the mixing media. Mixed powders were calcined at 700°C for 6 h. Dense pellets of the calcined powders were sintered at 1100°C for 3 h inside closed crucibles with powders of the identical compositions spread around to minimize the loss of volatile components from the pellets. The pellets so obtained were $\sim 96\%$ dense and the maximum weight loss was found to be $\sim 1\%$. For diffraction studies pellets were crushed with an agate mortar and pestle. The powders so obtained were annealed at 500°C . For dielectric studies, the surfaces of the sintered pellets were painted with silver paste and cured at 500°C for 30 min. A HP 4192 Impedance analyzer was used for capacitance and loss tangent measurements. The pellets were heated at the rate of 1°C min^{-1} by a programmable temperature controlled heater-cum-sample chamber. Neutron powder diffraction data at room temperature were collected at instrument SPODI, FRM II, Germany using a wavelength of 1.548 \AA . Synchrotron x-ray powder diffraction data were collected at different temperatures at instrument B2, HASYLAB, Germany using a wavelength of 0.5 \AA . Rietveld analysis was performed using the software package 'Fullprof' [33].

3. Results and discussion

3.1. Structures at room temperature

Figure 1 shows the synchrotron x-ray powder diffraction profiles patterns of the pseudocubic $\{111\}_{\text{pc}}$ and $\{200\}_{\text{pc}}$ peaks

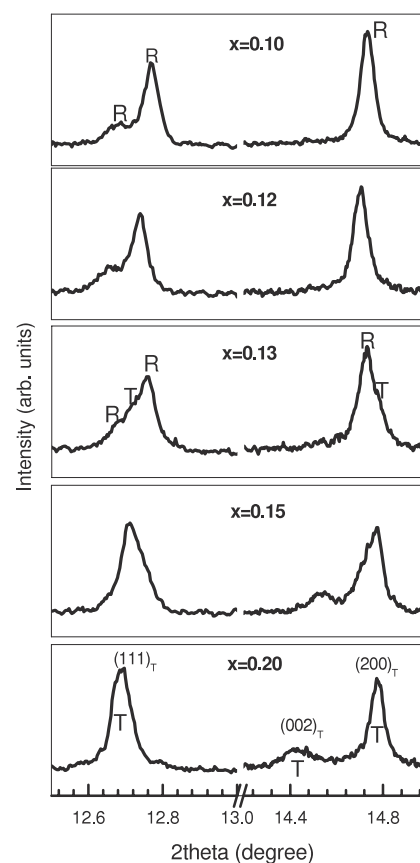


Figure 1. $\{111\}_{\text{pc}}$ (left) and $\{200\}_{\text{pc}}$ (right) pseudocubic x-ray powder diffraction profiles of $(1-x)\text{NBT-(x)PT}$ at room temperature. Labels R and T correspond to rhombohedral and tetragonal peaks, respectively.

of $(1-x)\text{NBT-(x)PT}$ of compositions near the MPB region. It is known that a rhombohedral distortion of a cubic lattice manifests in a powder diffraction pattern in terms of splitting of the cubic $\{hhh\}$ reflections into two, while retaining the singlet nature of $\{h00\}$. The reverse is true for tetragonal distortion of a cubic lattice. In view of this, the XRD patterns of $x = 0.10$ and 0.12 are compatible with rhombohedral distortion and that of $x = 0.20$ with a tetragonal distortion. With regard to perovskites, there are two common polar space groups, $R3m$ and $R3c$, compatible with the rhombohedral distortion. The structure corresponding to the $R3m$ space group is similar to the ground state ferroelectric structure of the classical ferroelectric BaTiO_3 . The structure corresponding to the $R3c$ space group, on the other hand, consists of an out-of-phase rotation/tilt of the oxygen octahedra (labelled as $a^-a^-a^-$ tilt in the Glazer's notation scheme [34, 35]) about the three fold axis of the rhombohedral cell. Such a tilt gives rise to superlattice reflections in the diffraction patterns with all-odd indices when indexed with respect to a doubled pseudocubic cell, i.e., $2a_{\text{pc}} \times 2b_{\text{pc}} \times 2c_{\text{pc}}$ [34, 35]. Since the intensity of the superlattice reflections is dependent on the magnitude of the tilt angle, for small tilt it becomes increasingly difficult to detect the superlattice reflections using x-ray diffraction techniques because of the relatively low scattering efficiency of oxygen for x-rays. Since no superlattice reflections could be

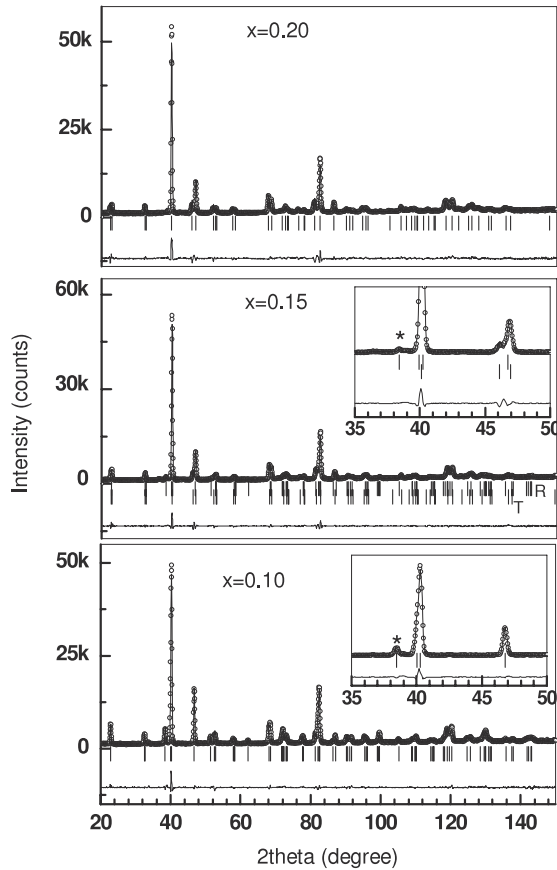


Figure 2. Rietveld plots of the neutron powder diffraction patterns of $(1-x)\text{NBT}-(x)\text{PT}$ at room temperature for $x = 0.10, 0.15$ and 0.20 . $x = 0.20$ and $x = 0.10$ were refined with tetragonal ($P4mm$) and rhombohedral ($R3c$) structures, respectively. The composition $x = 0.15$ was refined with two-phase ($R3c + P4mm$) model. The upper and lower vertical bars for $x = 0.15$ represent Bragg positions corresponding to the rhombohedral and tetragonal phases, respectively. The insets show magnified views in a limited 2θ range to highlight the weak superlattice reflection (marked with *).

detected in the XRD patterns of these samples, one could have concluded the rhombohedral structure with $R3m$ space group, as has been suggested in one of the earlier reports [25]. To ascertain the structure more reliably, we also collected neutron powder diffraction data on these samples because neutron diffraction is known to be successful in resolving structural issues related to very small magnitude of octahedral tilts in perovskites [36, 37]. The superlattice reflections, though of weak intensity, are clearly noticeable in the neutron powder diffraction data for $x \leq 0.15$. The insets of figure 2 show one of the superlattice reflections (marked with *) for $x = 0.10$ and 0.15 . This suggests that the correct space group of the rhombohedral phase for these compositions is $R3c$.

For $x = 0.13$, the $\{111\}_{\text{pc}}$ XRD profile shows features of three peaks suggesting the presence of tetragonal (labelled as T) and rhombohedral (labelled as R) phases (see figure 1). Although the broad features of the XRD Bragg profiles of $x = 0.15$ are suggestive of a tetragonal structure, the width of the $(111)_{\text{T}}$ and $(200)_{\text{T}}$ tetragonal peaks is comparatively larger than corresponding widths for $x = 0.20$. This suggests that $x = 0.15$ is also a mixture of tetragonal (major phase)

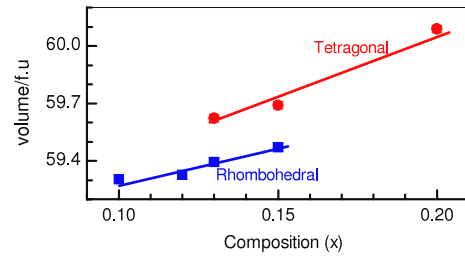


Figure 3. Variation of volume/f.u. of the tetragonal and rhombohedral phases with composition.

and rhombohedral (minor) phases. The presence of the weak superlattice reflection in the neutron diffraction pattern of $x = 0.15$ (see figure 2) further confirms the presence of the rhombohedral ($R3c$) structure. The continuance of the $R3c$ rhombohedral phase with increasing PbTiO_3 content contradicts the earlier suggestion by Park and Hong [25] that the superlattice phase ($R3c$) transforms to an untilted rhombohedral structure ($R3m$) with increasing concentration of PbTiO_3 . Rietveld refinement was therefore carried out with rhombohedral ($R3c$) structure for $x = 0.10$, and tetragonal (space group $P4mm$) structure for $x = 0.20$. For the rest of the compositions, two-phase (tetragonal + rhombohedral) refinement was done. The asymmetric unit of the tetragonal ($P4mm$) structure consists of one Na/Bi/Pb at $(0, 0, 0)$; one Ti at $(0.5, 0.5, 0.5 + \Delta_{\text{Ti}})$; one oxygen O1 at $(0.5, 0.5, 0 + \Delta_{\text{O1}})$ and another oxygen O2 at $(0, 0.5, 0.5 + \Delta_{\text{O2}})$ where the various Δ s represent refinable parameters. To avoid the floating origin, the coordinate of Na/Bi/Pb was fixed as origin. The rhombohedral ($R3c$) structure was described in terms of the convention used by Megaw and Darlington [38]. As per this description, the asymmetric unit of the structure consists of one Na/Bi/Pb at $0, 0, s + 0.25$, one Ti at $0, 0, 0 + t$, and one oxygen at $1/6 - 2e - 2d, 1/3 - 4d, 1/12$. The z -coordinate of oxygen was fixed at $1/12$ to avoid the problem of the floating origin in this structure. The octahedral tilt angle (ω) about the rhombohedral axis is defined as $\tan \omega = 4\sqrt{3}e$. Figure 2 shows representative Rietveld plots of $(1-x)\text{NBT}-x\text{PT}$ for $x = 0.10, 0.15$ and 0.20 . Table 1 lists the structural parameters of the compositions exhibiting pure rhombohedral ($x = 0.10$), pure tetragonal ($x = 0.20$) phase and a composition $x = 0.12$ in the phase coexistence region. As expected, for $x = 0.12$, the major phase was found to be rhombohedral ($\sim 77\%$). The fraction of the rhombohedral phase decrease drastically with x , and was found to be $\sim 65\%$ and $\sim 25\%$ for $x = 0.13$ and 0.15 , respectively. Figure 3 shows the variation of the volume/f.u. of the rhombohedral and tetragonal phases as a function of composition. It is evident from this plot that the volume of the tetragonal phase is higher by $\sim 0.2 \text{ \AA}^3$ as compared to the rhombohedral phase in the phase coexistence region. The discontinuous change in the volume, and the phase coexistence are suggestive of the first order nature of the $R3c$ - $P4mm$ structural transition.

3.2. Structural phase transition

The structural phase transition behaviour of $x = 0.10, 0.13, 0.15$ and 0.20 as a function of temperature was studied using

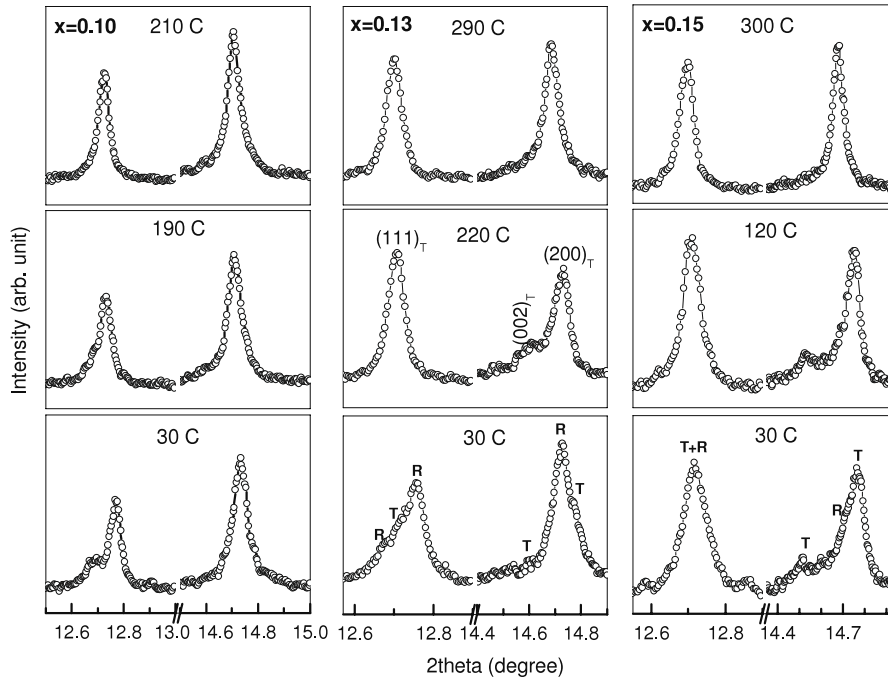


Figure 4. X-ray profiles of $\{111\}_{pc}$ and $\{200\}_{pc}$ pseudocubic reflections of $x = 0.10, 0.13$ and 0.15 at selected temperatures. The labels R and T denote positions of the peaks corresponding to the rhombohedral and tetragonal phases.

Table 1. Structural parameters of $(1-x)\text{NBT}-(x)\text{PT}$ at room temperature (from neutron data).

$x = 0.10$	$x = 0.12$		$x = 0.20$
(Space group $R3c$)	$R3c$	$P4mm$	(Space group $P4mm$)
Lattice parameters (\AA)			
$a_h = 5.4991(1)$	$a_h = 5.5006(1)$	$a = 3.8868(2)$	$a = 3.8887(2)$
$c_h = 13.5749(4)$	$c_h = 13.5797(5)$	$c = 3.9511(2)$	$c = 3.9735(4)$
Coordinates and atomic displacement parameters:			
$z_{\text{Na/Bi/Pb}} = 0.2738(2)$	$z_{\text{Na/Bi/Pb}} = 0.2744(2)$	$B_{\text{Na/Bi/Pb}} = 2.29 \text{ \AA}^2$	$B_{\text{Na/Bi/Pb}} = 2.12(9) \text{ \AA}^2$
$B_{\text{Na/Bi/Pb}} = 2.06(6) \text{ \AA}^2$	$B_{\text{Na/Bi/Pb}} = 2.09(5) \text{ \AA}^2$		
$z_{\text{Ti}} = 0.0109(3)$	$z_{\text{Ti}} = 0.0118(3)$	$z_{\text{Ti}} = 0.536$	$z_{\text{Ti}} = 0.537(1)$
$B_{\text{Ti}} = 0.94(5) \text{ \AA}^2$	$B_{\text{Ti}} = 0.94(5) \text{ \AA}^2$	$B_{\text{Ti}} = 0.74 \text{ \AA}^2$	$B_{\text{Ti}} = 0.74(9) \text{ \AA}^2$
$x_{\text{O}} = 0.1283(3)$	$x_{\text{O}} = 0.1302(3)$	$z_{\text{O1}} = 0.082$	$z_{\text{O1}} = 0.093(1)$
$y_{\text{O}} = 0.3336(5)$	$y_{\text{O}} = 0.3341(5)$	$B_{\text{O1}} = 1.97 \text{ \AA}^2$	$B_{\text{O1}} = 1.07(8) \text{ \AA}^2$
$z_{\text{O}} = 1/12$	$z_{\text{O}} = 1/12$	$z_{\text{O2}} = 0.589$	$z_{\text{O2}} = 0.604(1)$
$B_{\text{O}} = 1.32(2) \text{ \AA}^2$	$B_{\text{O}} = 1.28(2) \text{ \AA}^2$	$B_{\text{O2}} = 1.98 \text{ \AA}^2$	$B_{\text{O2}} = 1.35(6) \text{ \AA}^2$
Tilt angle $\omega = 7.6^\circ$	$\omega = 7.2^\circ$		
	% $R3c = 83$	% $P4mm = 17$	
$R_{wp}: 5.49$ $R_{exp}: 2.12$	$R_{wp}: 5.78$ $R_{exp}: 1.87$	$R_{wp}: 8.19$ $R_{exp}: 2.17$	

synchrotron XRD data. Figure 4 show profiles of pseudocubic $\{111\}_{pc}$ (at $2\theta \sim 12.7^\circ$) and $\{200\}_{pc}$ (at $2\theta \sim 14.7^\circ$) at three representative temperatures for $x = 0.10, 0.13, 0.15$. For $x = 0.10$, which is pure rhombohedral ($R3c$) at room temperature, the rhombohedral distortion of the lattice, as manifested in terms of separation of the two peaks of the $\{111\}_{pc}$ doublet, decreases with increasing temperature. At 210°C all the Bragg profiles of $x = 0.10$ became singlet, suggesting cubic structure. Thus $x = 0.10$ undergoes a rhombohedral ($R3c$)–cubic ($Pm3m$) transition in the temperature range $190^\circ\text{C} < T \leq 210^\circ\text{C}$. Similarly, the pure tetragonal composition, $x = 0.20$, shows a tetragonal ($P4mm$)–cubic ($Pm3m$) transition

at $\sim 370^\circ\text{C}$. On heating $x = 0.13$, which, as explained in section 3.1, has rhombohedral as the majority and tetragonal as the minority phase, the intensity of the peaks corresponding to the tetragonal ($P4mm$) phase (labelled as T in figure 4), increases with increasing temperature. For example, the $(002)_T$ tetragonal peak at $2\theta \sim 14.6^\circ$ which is nearly invisible at 30°C becomes noticeable at 220°C . Concomitantly, the intensity of the rhombohedral peaks decreases with increasing temperature. At 220°C the singlet nature of the $\{111\}_{pc}$ pseudocubic and the doublet nature of the $\{200\}_{pc}$ pseudocubic peaks of $x = 0.13$ is consistent with a pure tetragonal ($P4mm$) structure. On further heating the tetragonal distortion decreases

with temperature and finally becomes cubic. Similar features were observed for $x = 0.15$, for which the major phase at room temperature is tetragonal. This analysis suggests that for the compositions showing two phases (rhombohedral + tetragonal) at room temperature, the rhombohedral phase gradually transforms to the tetragonal phase on heating. The temperature variation of lattice parameters and phase fractions were obtained by Rietveld analysis of the XRD data, and are plotted in figure 5. For sake of direct comparison with the tetragonal lattice parameters, the hexagonal lattice parameters, a_h and c_h , of the rhombohedral phase are divided by $\sqrt{2}$ and $2\sqrt{3}$, respectively, to yield equivalent pseudocubic lattice parameters a_R^{pc} and c_R^{pc} . For an ideal cubic structure $a_R^{pc} = c_R^{pc}$. Further, similar to the spontaneous tetragonal strain defined as $(c/a - 1)$, the spontaneous lattice strain associated with the rhombohedral phase can be defined as $(c_R^{pc}/a_R^{pc} - 1)$.

For pure PbTiO_3 , it is known that the tetragonal strain exhibits a discontinuous jump, characteristic of a first order phase transition, at the cubic–tetragonal phase transition temperature. In contrast, the tetragonal structure of $x = 0.20$ exhibits a continuous development of the tetragonal strain below the cubic–tetragonal phase transition temperature (see inset of figure 5(a)). The tetragonal strain follows $A(T_C - T)^\nu$ dependence, and the best fit line along with the best fit parameters are shown in the inset of figure 5(a). Within error, the exponent ν was found to be ~ 0.5 . In the framework of mean field theory the strain is expected to follow a square dependence of the primary order parameter (spontaneous polarization in the case of ferroelectric transition). This would mean that the exponent corresponding to the temperature dependence of the primary order parameter (spontaneous polarization) would be $\nu/2$, i.e. ~ 0.25 . Such a value of exponent is known for systems exhibiting tricritical behaviour [39]. Similar analysis of the temperature dependence of rhombohedral strain leads to a curve shown in the inset of figure 5(d). The absolute values of the rhombohedral strain for $x = 0.10$ is an order of magnitude smaller than the tetragonal strain for $x = 0.20$. However, close to the transition temperature the rhombohedral strain drops much faster with temperature than the tetragonal strain. The exponent $\nu = 0.17$ (see inset of figure 5(d)) obtained by least squares fitting of strain–temperature cannot be rationalized in terms of mean field theory. We may attribute the relatively sharp drop of the rhombohedral strain near the transition temperature to the tendency of the system ($x = 0.10$) to undergo a first order transition, though the volume (per f.u.), as can be seen in the right inset of figure 5(d), does not show any noticeable discontinuous jump at the transition temperature.

For the compositions $x = 0.13$ and 0.15 , showing tetragonal ($P4mm$) + rhombohedral ($R3c$) phase mixture at room temperature, two-phase Rietveld analysis was carried out at various temperatures. Figures 5(b) and (c) show the temperature variation of the lattice parameters of both the phases as well as the phase fraction of the rhombohedral phase. As with the $x = 0.10$ case, the lattice parameters of the rhombohedral phase have been scaled for easy comparison with the lattice parameters of the tetragonal phase. The insets

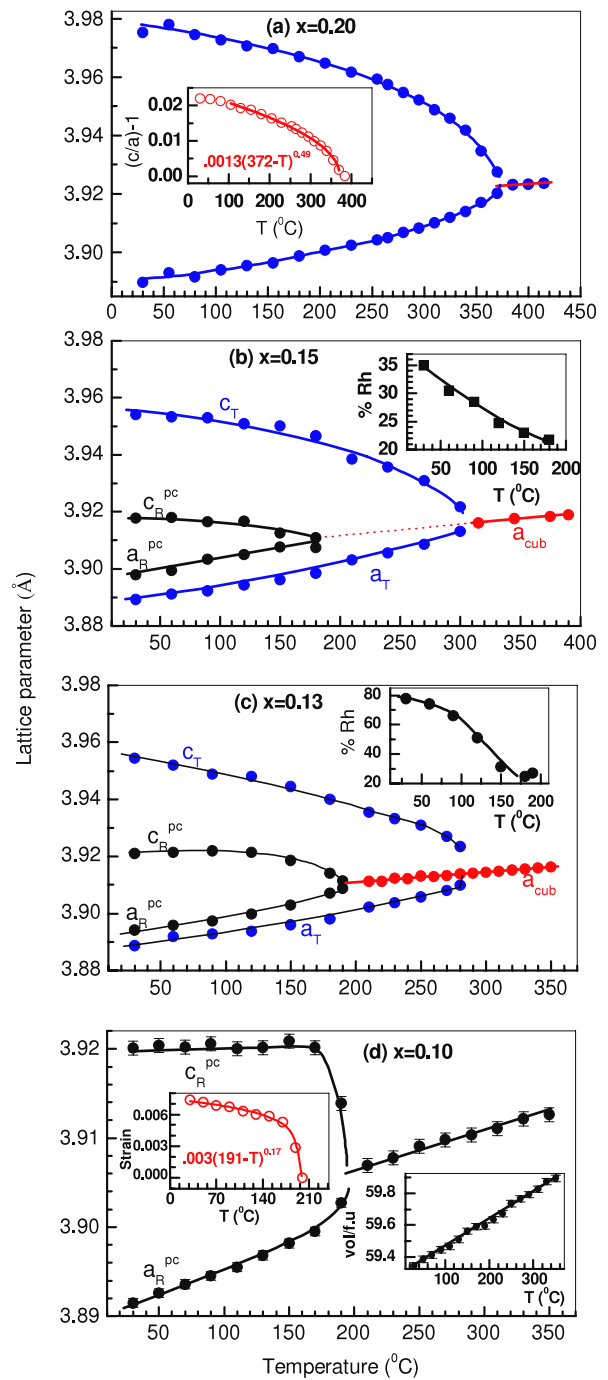


Figure 5. Temperature dependence of the tetragonal (a_T , c_T) and scaled rhombohedral (a_R^{pc} , c_R^{pc}) lattice parameters (see text) of (a) $x = 0.20$, (b) $x = 0.15$, (c) $x = 0.13$ and (d) $x = 0.10$. The lines through the data points are guides to eyes. The inset in (a) shows the temperature dependence of the spontaneous tetragonal strain. The continuous line in the inset corresponds to a fit as per the equation shown in the inset. The insets in (b) and (c) show the temperature variation of the rhombohedral phase fraction. The left inset in (d) shows the temperature variation of rhombohedral strain along with the fitted line and the equation. The right inset in (d) shows the temperature variation of the volume/f.u. in the rhombohedral and cubic phases.

of both the figures (5(b) and (c)) show a gradual decrease of the fraction of the rhombohedral phase with increasing temperature suggesting transformation of the rhombohedral

phase to the tetragonal phase, as mentioned in the beginning of this section. However, the rhombohedral distortion, as measured in terms of the difference between a_R^{pc} and c_R^{pc} , vanishes above $\sim 190^\circ\text{C}$ for $x = 0.13$ and above $\sim 180^\circ\text{C}$ for $x = 0.15$. This implies that the rhombohedral to tetragonal transformation takes place only below these temperatures for these compositions. At temperatures higher than these, the remaining rhombohedral phase transforms to cubic. There is, therefore, a temperature interval in which the system consists of tetragonal ($P4mm$) and cubic ($Pm3m$) phases. The tetragonal phase finally transforms to the cubic phase at $\sim 285^\circ\text{C}$ and $\sim 305^\circ\text{C}$ for $x = 0.13$ and 0.15 , respectively (see figures 5(b) and (c)). It is interesting to note that despite cubic phases forming at two different temperatures from two different non-cubic (rhombohedral and tetragonal) structures, the temperature dependence of their lattice parameters follow the same straight line. This feature maintains the overall phase integrity of the system at high temperatures. Otherwise the system would have ended up having two different cubic structures with different lattice parameters.

3.3. Dielectric behaviour

Figure 6 shows the temperature variation of the real (ϵ') and imaginary (ϵ'') parts of the relative permittivity of the four compositions, $x = 0.10, 0.13, 0.15$ and 0.20 at 1 kHz. For $x = 0.10$, the real part shows a well defined shoulder at $\sim 190^\circ\text{C}$, followed by a broad peak at 320°C . The imaginary part of this composition shows a peak at the same temperature (190°C) at which the shoulder appears in the real part. Since this temperature is identical to the rhombohedral–cubic structural phase transition temperature (190°C) of this composition (see figure 5(d)), the dielectric anomalies at 190°C are therefore attributed to the ferroelectric (rhombohedral, $R3c$)–paraelectric (cubic, $Pm3m$) phase transition. Broad anomalies are seen in the $\epsilon''(T)$ plots for the higher compositions as well, as shown in figure 6(b). However, unlike for $x = 0.10$, the anomalies corresponding to the higher compositions do not have anomalies in their respective $\epsilon'(T)$ counterparts. Furthermore, these anomalies were no longer visible for frequencies beyond 10 kHz, and hence may be associated with the relaxation of electrode–dielectric interfacial polarization. The broad anomaly in the real part of $x = 0.10$ at 320°C is similar to what has been reported earlier for pure $\text{Na}_{0.5}\text{Bi}_{0.5}\text{TiO}_3$ [15]. Earlier investigators have associated this anomaly to an antiferroelectric–paraelectric transition [14]. The antiferroelectric state has been associated with a coexistence of rhombohedral and a different type of tetragonal ($c/a = 1.003$) phases [14]. As discussed above, our results do not show evidence of noticeable tetragonal distortion above the temperature corresponding to the disappearance of the rhombohedral phase (190°C) for $x = 0.10$, thereby suggesting that the rhombohedral phase transforms directly to cubic above 190°C . The broad dielectric anomaly at 320°C for $x = 0.10$, therefore occurs in a globally cubic phase, and hence may be attributed either (i) to relaxation of superparaelectric clusters proposed earlier by Tu *et al* [15] or (ii) to space charge polarization due to high conductivity losses at these temperatures (see figure 6(b)).

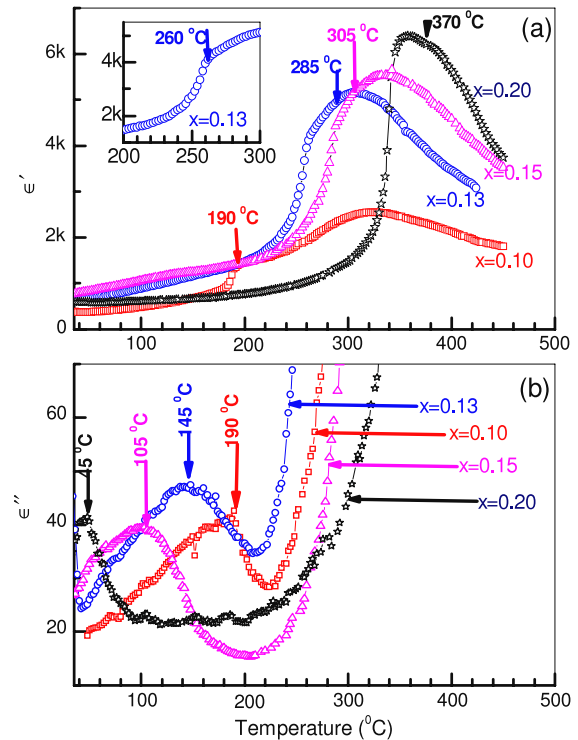


Figure 6. Temperature dependence of the (a) real part (ϵ') and (b) imaginary part (ϵ'') of the relative permittivity of $x = 0.10, 0.13, 0.15$ and 0.20 at 1 kHz. The arrows in (a) indicate the structural phase transition temperatures as obtained from the x-ray powder diffraction analysis (see text). The inset in (a) shows a magnified plot of $x = 0.13$ in a limited temperature range. The arrows in (b) indicate the temperatures corresponding to the maxima.

The $\epsilon'(T)$ plot of $x = 0.13$ and 0.15 shows two distinct anomalies. The one at lower temperature is characterized by a sudden change in the slope of the $\epsilon'(T)$ curve. This is more clearly revealed for $x = 0.13$, for which this anomaly occurs at 260°C , as shown in the inset of figure 6(a). The corresponding anomaly for $x = 0.15$ occurs at $\sim 290^\circ\text{C}$. Similar anomalies were earlier reported by Park and Hong [25] and Sakata *et al* [24] and were attributed to the rhombohedral–tetragonal transition. In view of the fact that the transformation of the rhombohedral ($R3c$) phase to the tetragonal ($P4mm$) phase occurs gradually with increasing temperature above room temperature, and that the rhombohedral phase survives along with the tetragonal phase only until $\sim 180^\circ\text{C}$ for $x = 0.13$ and $\sim 190^\circ\text{C}$, for $x = 0.15$, the dielectric anomaly at 260°C cannot be attributed to the rhombohedral–tetragonal transition proposed earlier [24, 25]. With the x-ray powder diffraction data, it is not possible to comment on any possible association of this dielectric anomaly with subtle structural changes, if any. Careful neutron powder diffraction and electron diffraction studies may, perhaps, throw more light on this issue. The second, and more obvious anomalies in figure 6(a), correspond to the diffuse maxima of the $\epsilon'(T)$ plots. For $x = 0.13, 0.15$ and 0.20 , these maxima occur at $303^\circ\text{C}, 335^\circ\text{C}$ and 355°C , respectively. For the sake of comparison, the tetragonal–cubic transition temperatures of these compositions, as obtained by the x-ray powder diffraction data, are indicated by arrows on the corresponding $\epsilon'(T)$ plot. It is evident that for

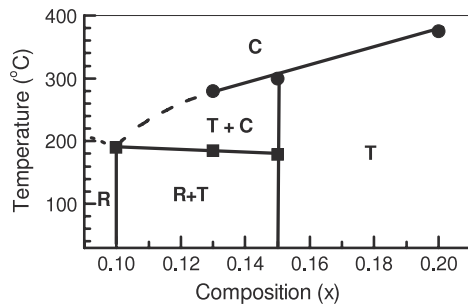


Figure 7. Phase diagram of $(1-x)\text{NBT}-(x)\text{PT}$ for compositions close to the MPB. The labels R, T, and C denote rhombohedral, tetragonal and cubic phases, respectively.

$x = 0.13$ and 0.15 the tetragonal (ferroelectric)–cubic (paraelectric) transition occurs at temperatures between the two dielectric anomalies. For $x = 0.20$, it lies above the diffuse maximum temperature. This analysis, therefore, suggests that the diffuse maxima in figure 6(a) do not represent the ferroelectric (tetragonal)–paraelectric (cubic) transition temperatures of these compositions. It may rather be a resultant of a superposed influence of (i) sudden rise in the relative permittivity due to the ferroelectric–paraelectric transition and (ii) dielectric relaxation, presumably Maxwell–Wagner type, due to sharp increase in the dielectric loss at high temperatures (see figure 6(b)).

4. Conclusions

In conclusion, a detailed study of the structural phase transition behaviour of the MPB compositions of the NBT–PT system has revealed that the MPB consists of rhombohedral ($R3c$) + tetragonal ($P4mm$) phases with the fraction of tetragonal phase increasing with the PbTiO_3 content. The rhombohedral phase just outside the MPB region ($x = 0.10$) transforms directly to cubic above a critical temperature. This transition is also characterized by a dielectric anomaly in the real and the imaginary parts of the relative permittivity. For the MPB compositions, $x = 0.13$ and 0.15 , irrespective of the dominant phase present at room temperature, the rhombohedral phase invariably transforms to tetragonal ($P4mm$) on heating. Both the rhombohedral and the tetragonal phases transform separately to cubic at different temperatures. A phase diagram depicting the different phase fields of the compositions near the MPB is shown in figure 7. The dielectric maxima of $x = 0.13$, 0.15 and 0.20 do not correspond to the ferroelectric (tetragonal, $P4mm$)–paraelectric (cubic, $Pm3m$) transition temperature, but rather seem to be a resultant of a superposition of the enhanced relative permittivity associated with the ferroelectric–paraelectric transition and space charge relaxation due to considerable enhancement of the dielectric loss at high temperatures.

References

- [1] Uchino K 2000 *Ferroelectric Devices* (New York: Dekker)
 [2] Jaffe B, Cook W R and Jaffe H 1971 *Piezoelectric Ceramics* (New York: Academic)

- [3] Noheda B 2002 *Curr. Opin. Solid State Mater. Sci.* **6** 27
 [4] Noheda B, Cox D E, Shirane G, Guo R, Jones B and Cross L E 2000 *Phys. Rev. B* **63** 014013
 [5] Hatch D M, Stokes H T, Ranjan R, Ragini, Mishra S K, Pandey D and Kennedy B J 2002 *Phys. Rev. B* **65** 212101
 [6] Kiat J M, Uesu Y, Dkhil B, Matsuda M, Malibert C and Calvarin G 2002 *Phys. Rev. B* **65** 064106
 [7] Singh A K and Pandey D 2003 *Phys. Rev. B* **67** 064102
 [8] Singh A K and Pandey D 2003 *Phys. Rev. B* **68** 172103
 [9] Noheda B, Cox D E, Shirane G, Gao J and Ye Z-G 2002 *Phys. Rev. B* **66** 054104
 [10] La-Orautapong D, Noheda B, Ye Z-G, Gehring P M, Toulouse J, Cox D E and Shirane G 2002 *Phys. Rev. B* **65** 144101
 [11] Smolenski G A, Isupov V A, Agronovskaya A I and Kainik N N 1961 *Sov. Phys.—Solid State* **2** 2651
 [12] Vakhrushev S B, Ivanitskii B G, Kvyatkovskii B E, Maisternko A N, Malysheva R S, Okuneva N M and Parfenova N N 1983 *Fiz. Tverd. Tela* **25** 2613
 [13] Vakhrushev S B, Ivanitskii B G, Kvyatkovskii B E, Maisternko A N, Malysheva R S, Okuneva N M and Parfenova N N 1983 *Sov. Phys.—Solid State* **25** 1504 (Engl. Transl.)
 [14] Zvirgzds J A, Kapostins P P and Zvirgzde J V 1982 *Ferroelectrics* **40** 75
 [15] Pronin I P 1985 *Ferroelectrics* **63** 153
 [16] Tu C-S, Siny I G and Schmidt V H 1994 *Phys. Rev. B* **49** 11550
 [17] Suchanicz J and Kwapulinski J 1995 *Ferroelectrics* **195** 249
 [18] Jones G O and Thomas P A 2002 *Acta Crystallogr. B* **58** 168
 [19] Jones G O and Thomas P A 2000 *Acta Crystallogr. B* **56** 426
 [20] Chiang Y M, Farrey G W and Soukhovjak A N 1998 *Appl. Phys. Lett.* **73** 3683
 [21] Takenaka T, Maruyama K and Sakata K 1991 *Japan. J. Appl. Phys.* **30** 2236
 [22] Hosono Y, Harada K and Yamashita Y 2001 *Japan. J. Appl. Phys.* **40** 5722
 [23] Ranjan R and Dwivedi A 2005 *Solid State Commun.* **135** 394
 [24] Elkechai O, Marchel P, Thomas P, Manier M and Mercurio J P 1997 *J. Mater. Chem.* **7** 91
 [25] Sakata K, Takenaka T and Naitou Y 1992 *Ferroelectrics* **131** 219
 [26] Park S E and Hong K S 1996 *J. Appl. Phys.* **79** 383
 [27] Hong K S and Park S E 1996 *J. Appl. Phys.* **79** 388
 [28] Said S, Marchet P, Merie-Mejean T and Mercurio J-P 2004 *Mater. Lett.* **58** 1405
 [29] Sakata K and Masuda Y 1974 *Ferroelectrics* **7** 347
 [30] Park S E and Hong K S 1997 *J. Mater. Res.* **12** 2152
 [31] Ishii H, Nagata H and Takenaka T 2001 *Japan. J. Appl. Phys.* **40** 5660
 [32] Wada T, Toyoiike K, Imanaka Y and Matsuo Y 2001 *Japan. J. Appl. Phys.* **40** 5703
 [33] Takenaka T, Sakata K and Toda K 1990 *Ferroelectrics* **106** 375
 [34] Rodrigues-Carvajal J 2000 FULLPROF A Rietveld Refinement and Pattern Matching Analysis Program Laboratoire Leon Brillouin (CEA-CNRS) France
 [35] Glazer A M 1972 *Acta Crystallogr. B* **28** 3384
 [36] Glazer A M 1975 *Acta Crystallogr. A* **31** 756
 [37] Ranjan R, Ragini, Mishra S K, Pandey D and Kennedy B J 2001 *Phys. Rev. B* **65** R060102
 [38] Ranjan R, Agrawal A, Senyshyn A and Boysen H 2006 *J. Phys.: Condens. Matter* **18** L515
 [39] Ranjan R, Agrawal A, Senyshyn A and Boysen H 2006 *J. Phys.: Condens. Matter* **18** 9679
 [40] Megaw H D and Darlington C N W 1975 *Acta Crystallogr. A* **31** 161
 [41] Strukov B A and Levanyuk A P 1997 *Ferroelectric Phenomena in Crystals* (Berlin: Springer)